Progress In Electromagnetics Research M, Vol. 117, 105–118, 2023

Design of High-Performance Parallel-Connected Filters Using Chained Filtering Functions

Francis E. Chinda[1, *], Socheatra Seoung[1], Muhammad S. Yahya[1], Sovuthy Cheab[2], and Huzein F. Hawari[1]

Abstract—This paper presents a design of high-performance parallel-connected filters using Chained filtering function. The filtering functions enable the placement of multiple return loss zeros at the same frequency, resulting in reduced sensitivity to fabrication tolerance and design complexity compared to traditional Chebyshev counterparts. To demonstrate the feasibility of this technique, a new filtering function (F_N) based on Chained filtering function is derived, and prototypes of fourth and sixth-degree Chained function filters in a parallel-connected topology are designed and fabricated. The overall size of the filters is 2.5 cm×4 cm (fourth degree) and 2.5 cm×5 cm (sixth degree). The measured insertion and return losses are 2.833 dB and 16.150 dB (fourth degree), and 2.674 dB and 18.074 dB (sixth degree). The achievable selectivity of the filters is 78.17 (fourth degree) and 89.68 (sixth degree). This design technique can serve as a useful tool for filter design engineers in terms of implementation.

1. INTRODUCTION

Parallel connected (PC) two-port chained function (CF) networks also identified as transversal and foster filters have been investigated and presented in [1, 2]. The network can be synthesized by rotating the submatrix in even/odd mode and grouping the residues [3, 4]. Computational methods were used to synthesize two branch parallel chained networks [5]. A transversal filter's admittance matrix was equated with a ladder network, and additional computations were performed to design a 4-pole transversal dielectric resonator filter [4]. The eigenmode expansion technique is applied to H and Z matrix for the even-mode degree to design foster types of networks in [6, 7]. This paper presents a straightforward and more generalized technique to design and synthesize such networks. Fourth and sixth-degree filter prototypes are fabricated to prove the feasibility of this approach. This paper is sequenced as follows. Section 2 presents the filtered theoretical analysis and synthesis techniques. Section 3 presents the design results and discussions including the filters prototypes and measured values. Section 4 provides the conclusion.

1.1. Contributions

1. This work introduced a new Chained filtering function for even and odd mode admittance, which can place multiple return loss zeros at the same frequency. This function can be used to design symmetrical and asymmetrical filters across various technologies and frequencies. It offers advantages in producing high-performance filters with reduced sensitivity. This will be a valuable mathematical tool for filter design engineers to simplify design and improve performance.

Received 25 November 2022, Accepted 13 May 2023, Scheduled 9 June 2023
* Corresponding author: Francis E. Chinda (Emmanuel_19000968@utp.edu.my).
[1] Department of Electrical and Electronic, Universiti Teknologi PETRONAS, Bandar Seri Iskandar, Perak 32610, Malaysia. [2] FILPAL (M) Snd Bhd,Bayan Lapas, Penang 11900, Malaysia.

2. This research introduces a new technique for realizing compact filter prototypes using open-loop resonators in parallel connected topology. This will significantly enhance the filter-tuning processes for faster production at a lower cost. The filter's compact size and improved tolerance properties make it a promising candidate for integration into front-end subsystems and deployment in wireless communication, satellite, and radar systems applications.

2. METHODOLOGY

This section provides detailed steps and techniques employed to achieve the design of the filters.

2.1. Formation of Chained Filtering Function

A Chained filtering function in this work can be formed by multiplying the Chebyshev polynomial function of the first kind. The seed function is generated in Maplesoft by using Eq. (1).

$$K_{i+1}(\omega) = 2\omega K_i(\omega) - K_{i-1}(\omega) \tag{1}$$

where $K_0(\omega) = 1$ and $K_1(\omega) = \omega$, while $i = 2, 3, \ldots, n_{s(k)}$ represent the coefficients seed function polynomial.

2.2. Seed-function Polynomial Selection

The transfer and reflection function responses were theoretically plotted for all possible seed functions for both fourth and sixth-order filters using Maplesoft Maple to predict the filter's performance in terms of transmission and reflection powers within the passband, while also maintaining a return loss value of 20 dB and a ripple factor (ε) of 0.1005. Based on the expected response, the seed function polynomials in Eqs. (1) and (2) were selected for the synthesis of fourth and sixth-order filters. Figs. 1 and 2 show the theoretical plots for 4th and 6th order CF filters.

$$F_N = 4\omega^4 - 4\omega^2 + 1 \tag{2}$$

$$F_N = 8\omega^6 + 12\omega^4 + 6\omega^2 - 1 \tag{3}$$

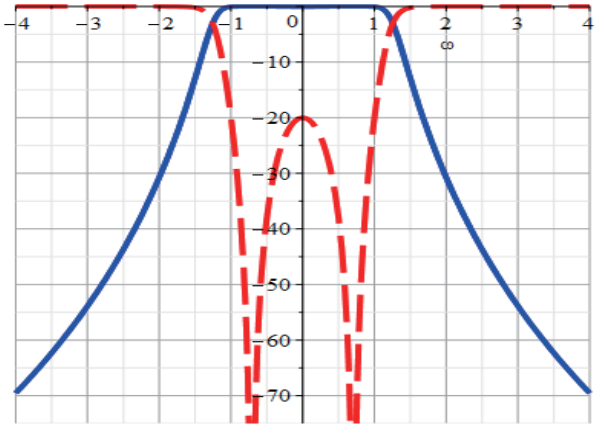

Figure 1. 4th order CF theoretical plot.

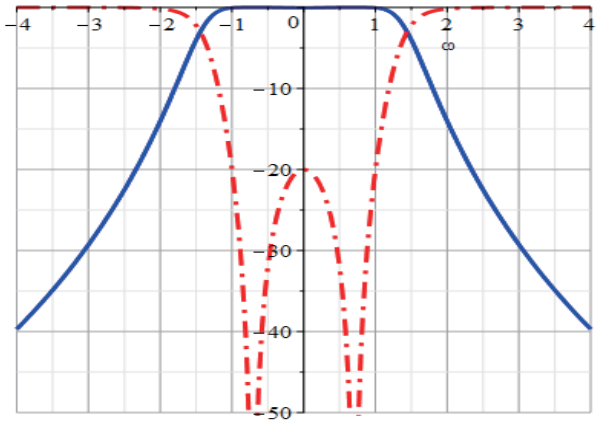

Figure 2. 6th Order CF theoretical plot.

2.3. The Parallel Connected Chained Function Filter Synthesis Technique

The technique for synthesizing parallel connected chained function filters involves using the even and odd mode admittance expressions of low-pass prototype networks [8]. These expressions allow for the creation of sub-branches that can be connected in parallel between the source and load. When being

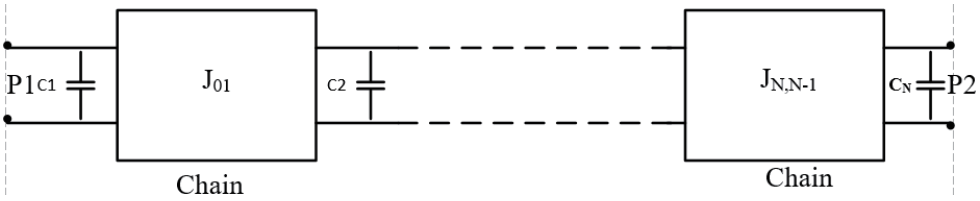

Figure 3. Inverter-coupled low-pass Chained function network.

combined, these sub-branches exhibit the same properties as a ladder network. The inverter network depicted in Fig. 3 can be synthesized by solving for the functions F_N, S_{11}, and S_{21}.

$$F_N = \frac{j}{2}\left(\prod_{r=1}^{N}\left\{\frac{1+hh_r+\left[\left(1+h^2\right)\left(1+h_r^2\right)\right]^{\frac{1}{2}}}{h-h_r}\right\}\right)+\prod_{r=1}^{N}\left\{\frac{1+hh_r-\left[\left(1+h^2\right)\left(1+h_r^2\right)\right]^{\frac{1}{2}}}{h-h_r}\right\} \tag{4}$$

$$|S_{11}(\omega)|^2 = \frac{\varepsilon^2 F_N^2(\omega)}{1+\varepsilon^2 F_N^2(\omega)} \tag{5}$$

$$|S_{21}(\omega)|^2 = \frac{1}{1+\varepsilon^2 F_N^2(\omega)} \tag{6}$$

where h, j, and p_r are the positions of transmission zeros (TZ), and N is the degree of the filter. The admittance of even-mode polynomial Y_e can be obtained by solving for the roots of $S_{11}(h)$ as described in [9, 10]. The transfer function matrix $ABCD$ for the filter can be formed using relevant expressions from [3, 21], and using partial fraction expansion allows for the placement of the resonators into a parallel network [12, 13].

$$S_{21}(p) = \frac{Y_e - Y_o}{(1+Y_e)(1+Y_o)} \tag{7}$$

$$S_{11}(p) = \frac{(1-Y_eY_o)}{(1+Y_e)(1+Y_o)} \tag{8}$$

2.4. Synthesis of Fourth Order Chained-Function Filter

The full synthesis technique of the fourth-order chained function is presented. The filtering function is formed by multiplying the Chebyshev seed function polynomial of the first kind [11]. The synthesis technique involves deriving the even and odd modes of admittance of the filter from Eq. (2). The synthesis steps are as follows.

Step 1: The S-parameters are used to derive the zeros in Eq. (9):

$$h^8 + 2h^6 + 1.5h^4 + 0.5h^2 + 6.25 = 0 \tag{9}$$

Step 2: The transfer function can be derived as a two-branch parallel network by formulating Y_e, the roots of S_{11}, and S_{11} is used to form the polynomial, $H(h)$ as in Eq. (10) [4].

$$1 + Y_e = 1 + \frac{N(h)}{D(h)} \tag{10}$$

Sep 3: The denominator can be factorized using partial fraction expression, and Y_e is split into two parts as.

$$Y_e'(h) = \frac{1}{1.080737547h + j0.8282225677} + \frac{1}{2.1578335886h - j3.301737005} \tag{11}$$

Step 4: The same approach can be used to generate the same results in the odd-mode admittance network.

$$Y_o(h) = \frac{1}{1.080737547h - j0.8282225677} + \frac{1}{2.1578335886h + j3.301737005} \tag{12}$$

The J-admittance values form the numerator, while the capacitance values form the denominator of this technique. Choosing multiple parallel branches is a potential advantage of this technique in filter design as it allows designers to place resonators freely in the network. This technique can be applied in the design of odd-mode symmetrical higher-order filter networks.

2.5. Synthesis of Sixth-Order Chained-Function Filter

The full synthesis procedure for a sixth-order parallel connected chained function filter is presented. The filtering function is synthesized to prove the feasibility of this approach in higher filter order targeting at achieving better performance and selectivity. The complete synthesis technique of the sixth-order filter is presented. The filtering function is formed by multiplying the Chebyshev seed function polynomial of the first kind. The synthesis technique is carried out by deriving the filter even and odd modes of admittance from Eq. (3). The synthesis steps guide is as follows.

Step 1: The even-mode impedance, Y_e, and Y_o can be derived using Eqs. (13)–(14), and the zeros can be calculated [21].

$$h^{12} + 3h^{10} + 3.75h^8 + 2.5h^6 + 0.9375p^2 + 0.1875h^2 + 1.5625 = 0 \tag{13}$$

Step 2: By using Eq. (9), the even mode admittance can be formed as in Eq. (13).

$$Y'_e(h) = \frac{h^3 - 0.6576446734ih^2 + 1.743053976h - 0.8291561977i}{1.555186313h^3 - 1.022759995i + 0.75000000} \tag{14}$$

Step 3: The denominator can be factorized using partial fraction expression and Y_e is split into two parts as.

$$Y'_e(h) = \frac{1}{1.982h - j0.8708} + \frac{1}{1.5534h + j1.9510} + \frac{1}{2.5456p + j3.7217} \tag{15}$$

Step 4: The same technique can be used on the odd mode admittance network; the same result is.

$$Y'_o(h) = \frac{1}{1.982h + j0.8708} + \frac{1}{1.5534h - j1.9510} + \frac{1}{2.5456h - j3.7217} \tag{16}$$

The numerator is the J-admittance values, and the denominator is the capacitance values. Fig. 4 shows the new parallel chained network formed for the sixth-order filter. The circuit simulation S-parameters response is presented in Fig. 5. By using bandpass transformation equations in [12, 13], the low-pass network can be converted into a band-pass filter.

2.6. The Circuit Simulation of Parallel Chained Function Filters

The J-admittance and capacitance values derived from Eqs. (11) and (15) are converted into schematic parallel low-pass networks for the fourth and sixth-order filters to assess their low-pass performance [14]. The low-pass schematic network of the filter is presented in Figs. 4 and 5, while Figs. 6 and 7 show the S-parameter performance. Table 1 provides an overview of the low-pass parameters of the network.

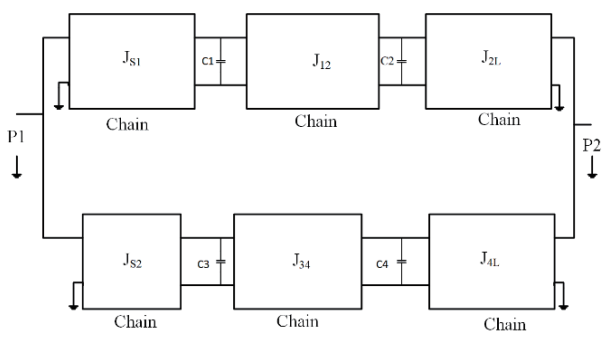

Figure 4. Fourth-order 2-branch LP layout.

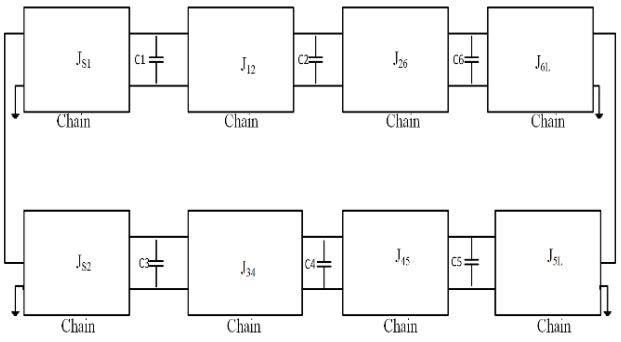

Figure 5. Sixth-order 2-branch LP layout.

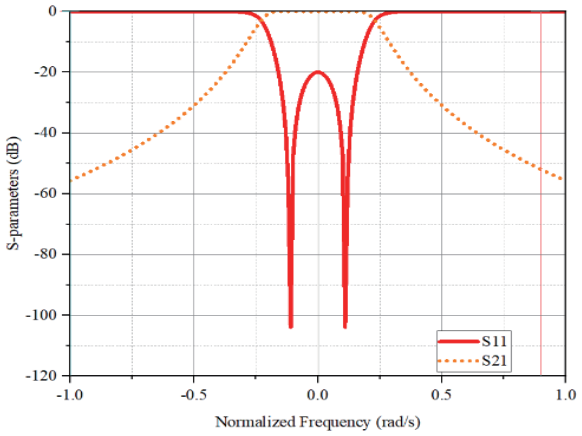

Figure 6. Fourth-order LP response.

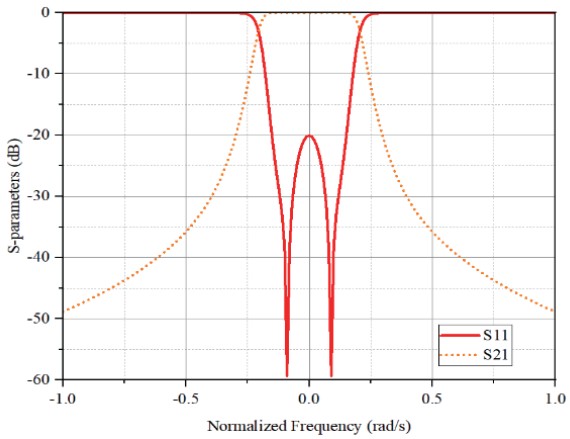

Figure 7. Sixth-order LP response.

Table 1. The fourth and sixth-order low-pass parameters.

Fourth order Parameters	{2,2}Seed Function	Sixth-order LP Parameters	{2,2,2}Seed Function
$C_1 = C_2$	1.0807F	$C_1 = C_6$	1.982F
$C_3 = C_4$	2.1578F	$C_2 = C_4$	1.553F
$J_{S1} = J_{2L}$	1	$C_3 = C_5$	2.546F
$J_{S3} = J_{4L}$	1	$J_{S1} = J_{S2} = J_{S3}$	1
J_{12}	0.8282	$J_{4L} = J_{5L} = J_{64}$	1
J_{34}	−3.3023	J_{16}	−0.8708
		J_{25}	1.9509
		J_{34}	−3.7217

2.7. The Parallel Chained Function Bandpass Transformation

The low-pass parameters of the filters are transformed into a bandpass filter by using the appropriate capacitive transformation equations in [15] and [16] to determine their performance in bandpass networks. Figs. 8 and 9 present the bandpass schematic layout of the filters, and Figs. 10 and 11 show its S-parameters performance. Table 2 summarizes the inductance and capacitance parameters of the bandpass filters.

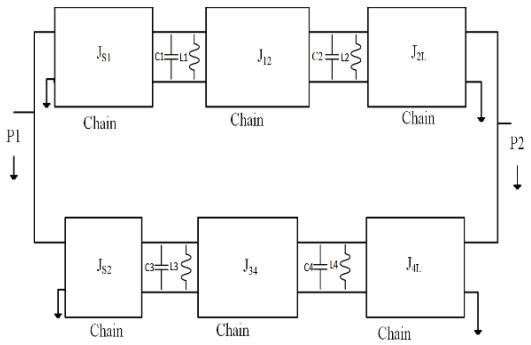

Figure 8. Fourth-order 2-branch BP layout.

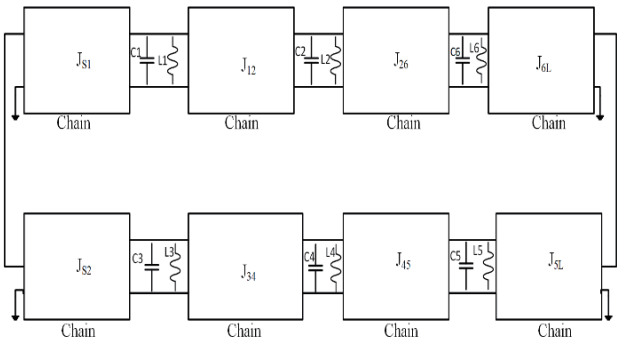

Figure 9. Sixth-order 2-branch BP layout.

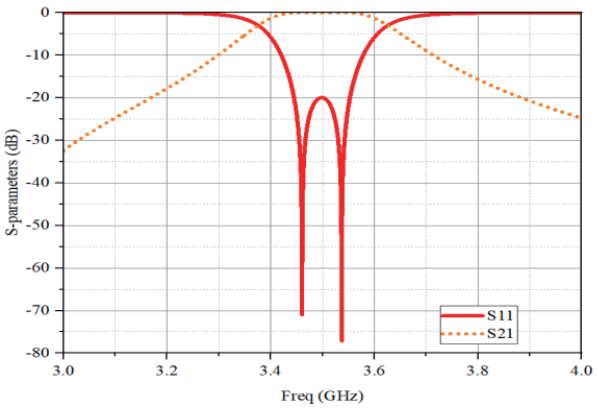

Figure 10. Fourth-order filter BP response.

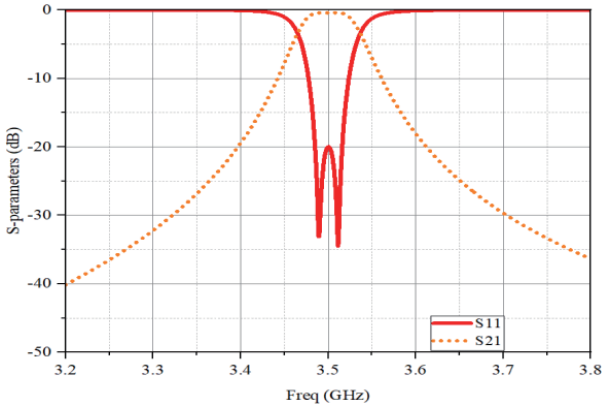

Figure 11. Sixth-order filter BP response.

The parallel bandpass filter networks for the fourth and sixth orders have generated two poles with a center frequency of 3.5 GHz and a return loss of 20 dB, as expected. This indicates a narrowband response and excellent performance in terms of signal reflection. The performance response aligns with the theoretical one, indicating consistency between the actual results and anticipated outcomes.

Table 2. Fourth and sixth-order bandpass parameters.

Fourth-order BP Parameters	{2,2}Seed Function	Sixth-order BP Parameters	{2,2,2}Seed Function
$L_1 = L_2$	0.002 nH	$L_1 = L_6$	1.014 nF
$L_3 = L_4$	1.014 nH	$L_2 = L_5$	0.0025 nF
$C_1 = C_2$	991.423 pF	$C_1 = C_6$	992 pF
$C_3 = C_4$	748.35 nH	$C_3 = L_4$	548.2 nH

2.8. Coupling Matrix Extractions

The process for obtaining the filters coupling matrix involves mapping and extracting it from the derived filtering function using the expressions in [17] and Eqs. (17) and (18). The transmission and reflection coefficients, S_{11} and S_{21}, are used to derive the coupling matrix for the filter network. Next, a similarity transformation and matrix element annihilation are performed to obtain the complete coupling matrix, M, as presented in [18–20]. This synthesized coupling matrix is then divided into subnetworks, and a series of configurations are carried out for the entire matrix until the desired coupling is achieved, as described in [17]. The full coupling matrix, M, for the fourth- and sixth-order filters is shown in Eqs. (19) and (20), which translate to $N + 2$ configurations and routing structures shown in Figs. 12 and 13.

$$S_{11}(\omega) = \frac{F_N(\omega)}{E_N(\omega)} \quad S_{21}(\omega) = \frac{P_N(\omega)}{\varepsilon E_N(\omega)} \tag{17}$$

$$y_{21}(s) = j\sum_{k=1}^{N} \frac{T_{Nk}T_{1k}}{\omega - \lambda_k} \quad y_{22}(s) = j\sum_{k=1}^{N} \frac{T_{Nk}^2}{\omega - \lambda_k} \tag{18}$$

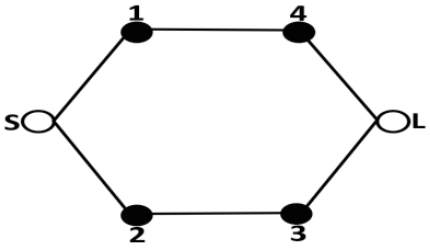

Figure 12. 4th-order filter routing topology.

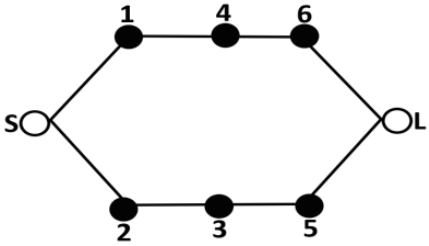

Figure 13. 6th-order filter routing topology.

where λ_k represents the pole of eigenvalue, and T_{1k} and T_{Nk} are the orthogonal first and last rows of the matrix T [21].

$$M = \begin{pmatrix} 0 & 0.68 & 0.96 & 0 & 0 & 0 \\ 0.68 & 0 & 0 & 0 & 1.53 & 0 \\ 0.96 & 0 & 0 & 0.77 & 0 & 0 \\ 0 & 0 & 0.77 & 0 & 0 & -0.96 \\ 0 & 1.53 & 0 & 0 & 0 & 0.68 \\ 0 & 0 & 0 & -0.96 & 0.68 & 0 \end{pmatrix} \tag{19}$$

$$M = \begin{pmatrix} 0 & 0.638 & 0.629 & 0.447 & 1.199 & 0 & 0 & 0 \\ 0.638 & 0 & 0 & 0 & 0 & 0 & 0 & 0 \\ 0.629 & 0 & 0 & 0 & 0 & 0 & 0 & 0 \\ 0 & 0 & -0.971 & 0 & 0 & -0.971 & 0 & 0 \\ 0 & 0.356 & 0 & 0 & 0 & 0 & 0.356 & 0 \\ 0 & 0 & 0 & 1.199 & 0 & 0 & 0 & 0.638 \\ 0 & 0 & 0 & 0 & 0.447 & 0 & 0 & 0.629 \\ 0 & 0 & 0 & 0 & 0 & 0.638 & 0.629 & 0 \end{pmatrix} \tag{20}$$

3. RESULTS AND DISCUSSION

3.1. Design and Simulation

This section presents the general overview of parallel-connected chained-function filter realization. The synthesized network can be realized on a microstrip if the Q-factor of the resonator is 300 or lower [21, 22]. An open loop microstrip resonator is chosen for this work because of its ease of tuning and inherent properties of reduced sensitivity. The simulation is carried out using an advance-design-system (ADS). The ideal circuit is then converted into a microstrip circuit by specifying the length and width of the resonators, as well as the loss and other parameters defining the microstrip properties [23]. In this stage, achieving a good inter-resonator coupling is based on extracting the external quality factor (Qe) and coupling coefficient (K) of the filters.

3.2. The Filters Inter-Resonators Coupling

The resonator coupling can be achieved by adjusting the gap or distance between the resonators. The coupling configuration between the adjacent resonators is a mixed coupling [24]. The values of the coupling coefficient (K) were obtained using the line calculation technique in ADS and Eq. (21) by carefully adjusting the gap and recording the resonant frequencies [1]. Table 3 presents the values of the coupling coefficient of the resonators, and Fig. 14 shows plots of the coupling coefficient versus the distance or gap (S) between the resonators.

$$M = \frac{f_0}{BW} \times \frac{f_2^2 - f_1^2}{f_2^2 + f_1^2} \tag{21}$$

Table 3. The coupling coefficient K versus S.

S (mm)	f_1 (GHz)	f_2 (GHz)	K
0.5	3.4490	3.6200	0.00674
1.0	3.5060	3.5940	0.03450
1.5	3.5320	3.5770	0.01760
2.0	3.5480	3.5630	0.00590

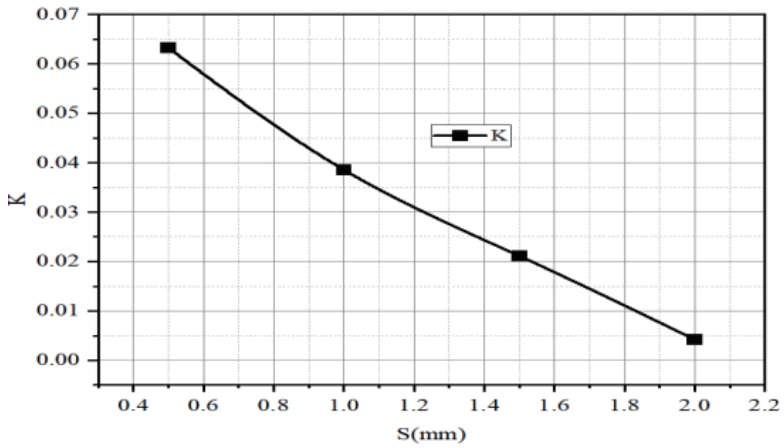

Figure 14. Coupling coefficient (K) versus the resonator gap (S).

The frequencies of the first and second eigenmodes are denoted by f_1 and f_2, while the center frequency is represented by f_0. M is the normalized coupling coefficient M; the coupling factor is K; and the filter bandwidth is BW.

3.3. The Filters Physical Layout Simulations

The synthesized low-pass admittance values for the filters are converted into an optimal physical network for realization [25]. The resonators are connected in parallel and chained to the filter output. Figs. 15 and 16 show the final physical layout of the filters, and Figs. 17 and 18 present the transmission and reflection S-parameters response.

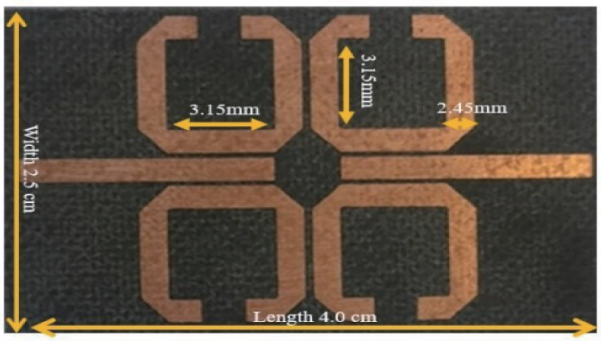

Figure 15. 4th-order parallel chained function (PCF) physical layout.

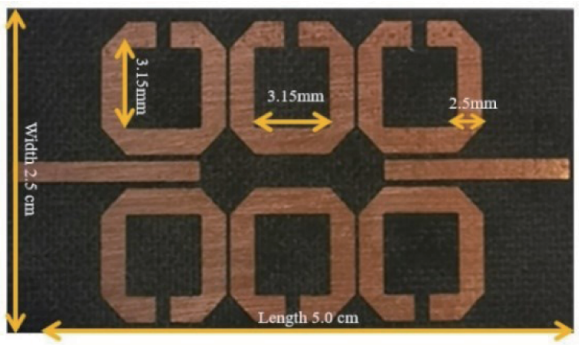

Figure 16. 6th-order PCF physical layout.

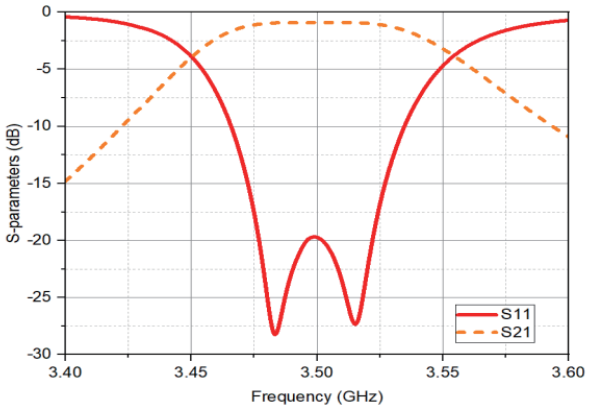

Figure 17. 4th order PCF response.

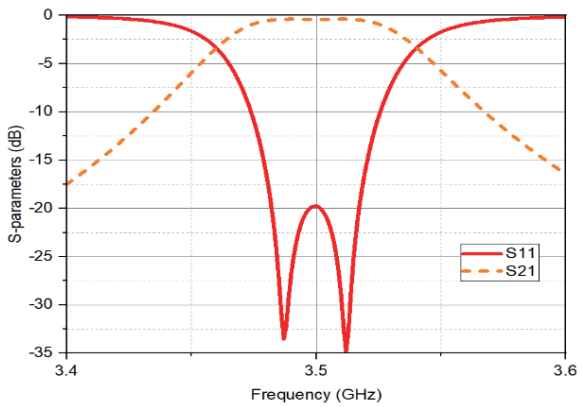

Figure 18. 6th order PCF response.

The filters have produced two poles in the passband as expected for chained function implementation. The fourth-order filter has achieved simulated insertion and return loss performances of 0.899 dB and 20 dB, the bandwidth and fractional bandwidth of 46.8 MHz and 1.34%, and a rejection of 14.9 dB, while the sixth-order filter has achieved simulated insertion and return losses of 0.409 dB/20 dB, the bandwidth and fractional bandwidth of 36.6 MHz and 1.045%, and a rejection of 18.03 dB. These results have been validated and are consistent with the theoretical response. The ability of Chained function polynomials in the placement of multiple filter return loss (RL) zeros at the same frequency is demonstrated. The simulation results have proven that the filter can provide good performance in terms of return loss, insertion loss, and out-of-band rejection levels.

3.4. The Filter Prototypes

The filter prototypes are fabricated on RT/Roger duroid 5880 substrates, with a thickness of 787 µm, a copper-clad thickness of 17.5 µm, a dielectric constant (ε_r) of 2.2, a loss tangent ($\tan\delta$) of 0.0009, and electrical length is 180°, which is equivalent to $\lambda/2$ [26, 27]. The dimensions of the filter resonator are 2.45 mm in width and 3.15 mm in length which were obtained using the expressions in [1]. The input and output ports of the filter are connected to SMA connectors with a size of 3.5 mm. The feed lines between the resonators and connectors are 10 mm. Figs. 19 and 20 present fabricated prototypes of the filter while the measured S-parameter performance is presented in Figs. 21 and 22.

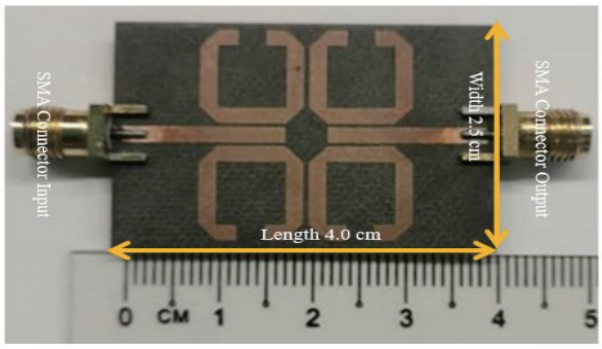

Figure 19. 4th-order PC filter prototype.

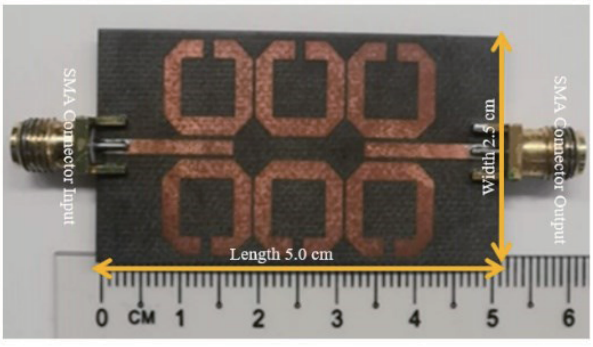

Figure 20. 6th-order PC filter prototype.

The filter's overall size is 2.5 cm×4 cm (fourth order) and 2.5 cm×5 cm (sixth order).

3.5. Comparison of the Filters Simulated and Measured Results

The simulated and measured results of the fourth- and sixth-order parallel connected Chained function filters are compared in terms of insertion loss, return loss, bandwidth, and out-out-of-band rejection performance as follows. Figs. 21 and 22 present the filter's simulated and measured transmission and reflection responses.

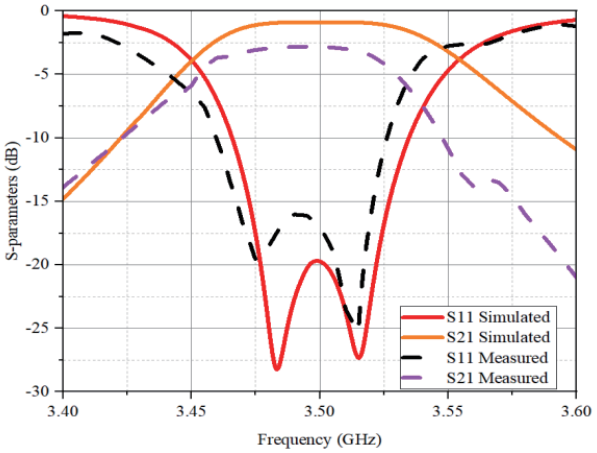

Figure 21. 4th order simulated/measured response.

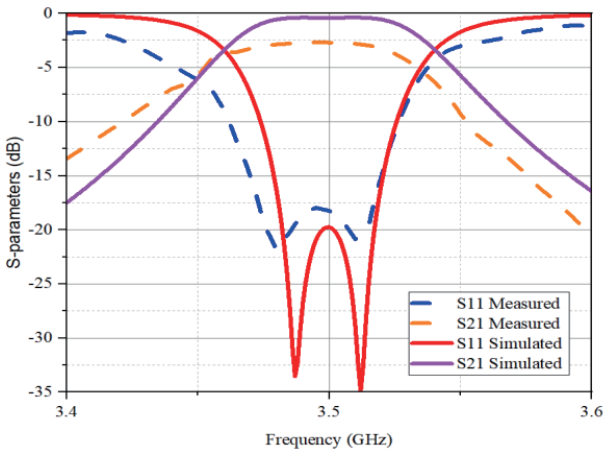

Figure 22. 6th order simulated/measured response.

The simulated and measured performances of the two filters are presented in this report. The first filter is a fourth order filter, which exhibits simulated and measured insertion/return losses of 0.899 dB/20 dB and 2.83 dB/16.150 dB. The simulated and measured bandwidths are 46.8 MHz and 50.4 MHz with fractional bandwidths (FBWs) of 1.34% and 1.44%. However, a small shift of 0.1% in the measured bandwidth was observed, which can be due to package parasitic effects, calibration cable loss, SMA soldering port and ground effects, or microstrip line junction radiation.

For the sixth order parallel connected Chained function filter, the simulated and measured insertion/return loss values are 0.396 dB/20 dB and 2.64 dB/18.03 dB. The simulated and measured bandwidths are 36.6 MHz and 44.1 MHz with FBWs of 1.045% and 1.262%. The filter exhibits good filtering performance. However, a small shift of 0.217% in the measured bandwidth was observed, which may be due to package parasitic effects, calibration cable loss, SMA soldering port and ground effects, or microstrip line junction radiation. These results indicate that the filters are compact and suitable for applications where high-performance filtering is required. The observed small shift in the measured bandwidth should be considered in the specific application.

3.6. Sensitivity Analysis

Sensitivity analysis is conducted on a parallel connected Chained function filter to prove and validate its fabrication tolerance [25, 28]. In this work, the analysis is carried out on the filter low-pass components values in ADS to check the impact of tolerance in the passband return loss levels. The values are modified to have a difference of (±1%, ±2%). The distribution's variance was chosen to provide a maximum tolerance of approximation as specified by the filter fabrication machines. Table 4 summarizes the filter tolerance parameters, while Figs. 23 to 26 present the performance of the filter when tolerance is applied.

The study found that higher applied tolerances can cause passband shifts in PC chained function filters. Tighter tolerances during fabrication result in lower filter sensitivity, leading to a more precise and predictable filter response. Using components with tight tolerances at the approximation stage and careful fabrication control can minimize sensitivity [15, 29]. The finding also confirmed that parallel-connected chained function filters are less sensitive to manufacturing errors, preserving selectivity. This

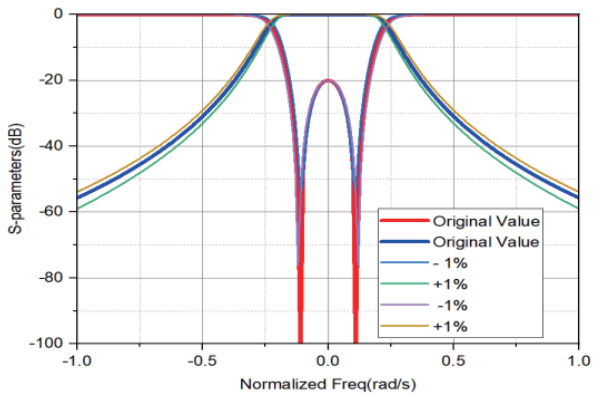

Figure 23. ±1% tolerance affects on 4th order filter.

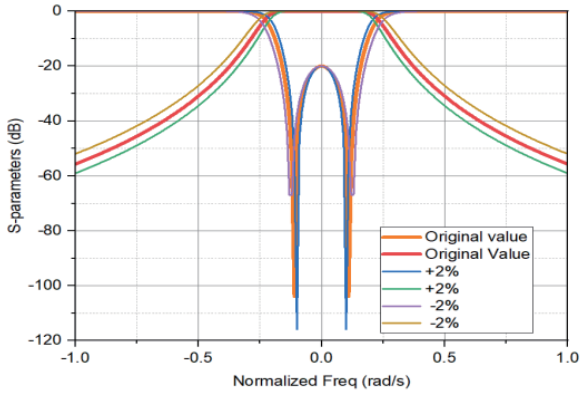

Figure 24. ±2% tolerance effects.

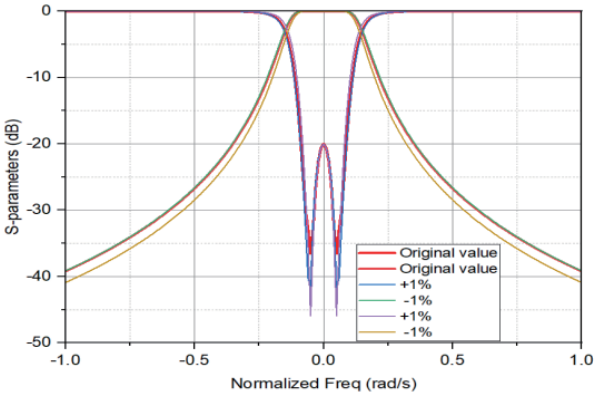

Figure 25. ±1% tolerance affects on 6th order filter.

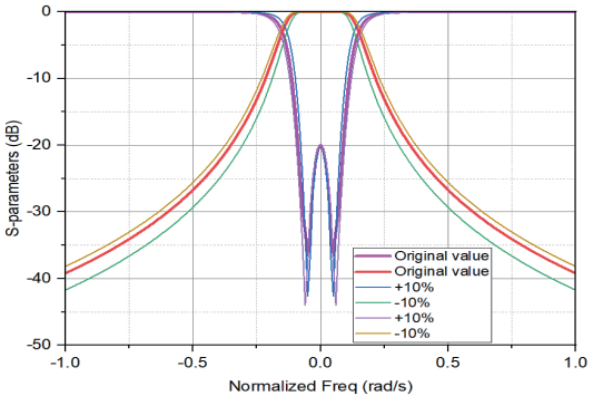

Figure 26. ±2% tolerance effects.

Table 4. Summary of tolerance impacts on the fourth and sixth-order pc chained filters.

4th order filter applied tolerance	RL Change (%)	6th order filter applied tolerance	RL Change (%)
−1%	2.60%	−1%	4.10%
+1%	9.42%	+1%	6.46%
−2%	8.5%	−2%	9.76%
+2%	12.62%	+2%	11.81%

is exhibited by the reduced percentage shift in RL zeros separations of the filters. The further apart separation of the filter poles is evident confirming higher manufacturing

3.7. Comparison with Related Work

Table 5 presents a comparison between the realized filters in this work and related research. This filter has achieved significant improvements in terms of selectivity insertion loss, return loss, rejection performance, and size compared to previous work. The reduced size of our filter makes it ideal for integration into wireless communication and front-end subsystems.

Table 5. Comparison of similar work.

Ref. Year	Filter order	Topology Type	Return Loss (dB)	Insertion Loss (dB)	BW (MHz)	Out-of-Band Rejection (dB)	Selectivity
[21]	4	Parallel	12.6	2	2.4	23	83.3
[22]	6	Series	14	2.8	624	30	8.33
[25]	5	Series	13	5.2	4.1	25	24
[17]	6	Series	13	2.7	480	25	8.33
[20]	4	Parallel	14	2.8	40	30	60
This work	4	Parallel	16.150	2.83	50.4	20.23	78.17
This work	6	Parallel	18.03	2.64	44.1	20.55	89.68

4. CONCLUSION

Fourth- and sixth-order prototypes of high-performance parallel-connected filters using Chained filtering functions were designed and fabricated. The overall size of the filters is 2.5 cm×4 cm (fourth order) and 2.5 cm×5 cm (sixth order). The achieved measured insertion/return loss is 2.83 dB/16.150 dB (fourth order) and 2.64 dB/18.074 dB (sixth order) filters. The selectivity obtained is 78.17 (fourth order) and 89.68 (sixth order). The theoretical and measured results were validated and are consistent with each other. The advantage of this filter prototype is that it offers reduced sensitivity and enhanced tuning processes while retaining performance comparable to conventional Chebyshev filters. The sensitivity analysis conducted on the filters has fully demonstrated their reduced sensitivity to manufacturing tolerance and proven their reliability. These filters are promising candidates for integration where high performance and selectivity are required. They can be used as a very useful design tool for any filter design engineer, as lower and higher-order filters can be implemented using chained function polynomials.

ACKNOWLEDGMENT

The authors would like to thank YUTP (015LC0-320) and collaborative research fund (015ME0-329) for providing the funding that allows this research to be viable and successful. The authors also appreciate all individuals who have contributed directly or indirectly to complete this project.

REFERENCES

1. Cameron, R. J., C. M. Kudsia, and R. R. Mansour, "Tunable filters," *Microw. Filters Commun. Syst.*, 731–783, 2018, doi: 10.1002/9781119292371.ch22.
2. Cameron, R. J., C. M. Kudsia, and R. R. Mansour, "Synthesis of networks: Direct coupling matrix synthesis methods," *Microw. Filters Commun. Syst.*, 247–294, 2018, doi: 10.1002/9781119292371.ch8.
3. Cameron, R. J., "Advanced coupling matrix synthesis techniques for microwave filters," *IEEE Trans. Microw. Theory Tech.*, Vol. 51, No. 1 I, 1–10, 2003, doi: 10.1109/TMTT.2002.806937.
4. Hunter, I. C., L. Billonet, B. Jarry, and P. Guillon, "Microwave filters — Applications and technology," *IEEE Trans. Microw. Theory Tech.*, Vol. 50, No. 3, 794–805, 2002, doi: 10.1109/22.989963.
5. Zhang, Y. and K. L. Wu, "General method for synthesizing dispersive coupling matrix of microwave bandpass filters," *Int. J. Microw. Wirel. Technol.*, Vol. 14, No. 3, 379–386, 2022, doi: 10.1017/S1759078721000672.

6. Pommier, V., D. Cros, P. Guillon, A. Carlier, and E. Rogeaux, "Transversal filter using whispering gallery quarter cut resonators," *IEEE MTT-S Int. Microw. Symp. Dig.*, Vol. 3, 1779–1782, 2000, doi: 10.1109/MWSYM.2000.862324.
7. Cameron, R. J., C. M. Kudsia, and R. R. Mansour, "Characterization of lossless lowpass prototype filter functions," *Microw. Filters Commun. Syst.*, 87–127, 2018, doi: 10.1002/9781119292371.ch3.
8. Lalbakhsh A., et al., "A design of a dual-band bandpass filter based on modal analysis for modern communication systems," *Electron.*, Vol. 9, No. 11, 1–13, 2020, doi: 10.3390/electronics9111770.
9. Ahn, K. P., A. Saitou, and K. Honjo, "Group delay analysis of differential-mode coupled four lines bandpass filters," *Asia-Pacific Microw. Conf. Proceedings, APMC*, Vol. 2, 1260–1263, 2006, doi: 10.1109/APMC.2006.4429635.
10. Perenić, G., N. Stamenković, N. Stojanović, and N. Denić, "Chained-function filter synthesis based on the modified jacobi polynomials," *Radioengineering*, Vol. 27, No. 4, 1112–1118, 2018, doi: 10.13164/re.2018.1112.
11. Wu, Y. and Q. Zeng, "A novel dual-band waveguide filter with multiple transmission zeros based on TE102- and TE103-modes," *IEEE Microw. Wirel. Components Lett.*, Vol. 32, No. 10, 1159–1162, 2022, doi: 10.1109/LMWC.2022.3175993.
12. Luhaib, S. W. O., M. S. Bakr, I. C. Hunter, and N. Somjit, "Compact triple-mode microwave dielectric resonator filters," *Int. J. Electron. Lett.*, 194–204, 2019, doi: 10.1080/00207217.2019.1582714.
13. Lim, Y. P., S. Cheab, S. Soeung, and P. W. Wong, "An the design and fabrication of chained-function waveguide filters with reduced fabrication sensitivity using CNC and DMLS," *Progress In Electromagnetics Research B*, Vol. 87, 39–60, 2020, doi: 10.2528/PIERB20011101.
14. Basheer, A., H. Abdulhussein, and J. K. Ali, "Design of bandpass filter for 5g applications with high-selectivity and wide band rejection," *2022 Muthanna International Conference on Engineering Science and Technology (MICEST)*, 179–183, 2022.
15. Liu, J., Y. X. Wang, G. Y. Wei, R. L. Jia, and Y. L. Duan, "Design of high-selective wideband bandpass filter with a notched-band and harmonic suppression," *Prog. Electromagn. Res. Lett.*, Vol. 105, 57–62, 2022, doi: 10.2528/PIERL22051001.
16. Zhang, Y., X. Shang, F. Zhang, and J. Xu, "A 3-D printed Ku-band waveguide filter based on novel rotary coupling structure," *IEEE Microw. Wirel. Components Lett.*, Vol. 33, No. 1, 35–38, 2022, doi: 10.1109/LMWC.2022.3194367.
17. Lim, Y. P., Y. L. Toh, S. Cheab, G. S. Ng, and P. W. Wong, "Chained-function waveguide filter for 5G and beyond," *IEEE Reg. 10 Annu. Int. Conf. Proceedings/TENCON*, 107–110, 2019, doi: 10.1109/TENCON.2018.8650548.
18. Wong, P. W., "A sustainable and fast approach to filter design for 5G implementation," *RFM 2018 — 2018 IEEE Int. RF Microw. Conf. Proc.*, Vol. 88, No. 3, 349–351, 2018, doi: 10.1109/RFM.2018.8846520.
19. Chappa, R., L. Janjanam, and S. K. Saha, "Performance analysis of optimal FIR LPF and HPF using AVOA," *2022 6th International Conference On Computing, Communication, Control And Automation (ICCUBEA*, 1–6, 2023, doi: 10.1109/iccubea54992.2022.10011081.
20. Lim, Y., S. Cheab, S. Soeung, and P. Wong, "On the design and fabrication of chained-function waveguide filters with reduced fabrication sensitivity using CNC and DMLS," *Progress In Electromagnetics Research B*, Vol. 87, No. May, 39–60, 2020.
21. Fernandez-Prieto, A., A. Lujambio, J. Martel, F. Medina, F. Martin, and R. R. Boix, "Balanced-to-balanced microstrip diplexer based on magnetically coupled resonators," *IEEE Access*, Vol. 6, 18536–18547, 2018, doi: 10.1109/ACCESS.2018.2820073.
22. Cheab, S., P. W. Wong, and X. Y. Chew, "Parallel connected dual-mode filter," *IEEE Microw. Wirel. Components Lett.*, Vol. 25, No. 9, 582–584, 2015, doi: 10.1109/LMWC.2015.2451393.
23. Al-Yasir, Y. I. A., N. O. Parchin, R. A. Abd-Alhameed, A. M. Abdulkhaleq, and J. M. Noras, "Recent progress in the design of 4G/5G reconfigurable filters," *Electron.*, Vol. 8, No. 1, 2019, doi: 10.3390/electronics8010114.

24. Mishra, V. and A. K. Sign, "Design and analysis of coupling matrix for microwave filter applications," *Int. J. Electr. Electron. Commun. Eng.*, Vol. 2, No. 7, 508–520, 2012.
25. Bong D. C. H., et al., "Analysis and design of a novel microstrip filter for C-band applications," *IEEE Access*, Vol. 7, No. 5, 130922–130936, 2019, doi: 10.1109/ICSSS.2019.8882868.
26. Tang, C. W. and J. M. Jiang, "Design of the microstrip bandpass filter with 4 band-switching modes," *IEEE Trans. Circuits Syst. II Express Briefs*, Vol. 3, 1–5, 2022, doi: 10.1109/TCSII.2022.3229105.
27. Cheab, S., P. W. Wong, and S. Soeung, "Design of multi-band filters using parallel connected topology," *Radioengineering*, Vol. 27, No. 1, 186–192, 2018, doi: 10.13164/re.2018.0186.
28. Lesnikov, V., T. Naumovich, and A. Chastikov, "Sensitivity analysis of digital filters using the continued fraction expansion," *2018 Moscow Workshop on Electronic and Networking Technologies (MWENT)*, 1–5, 2018, doi: 10.1109/MWENT.2018.8337178.
29. Zhao, K. and D. Psychogiou, "Single-to-multi-band reconfigurable acoustic-wave-lumped-resonator bandpass filters," *IEEE Trans. Circuits Syst. II Express Briefs*, Vol. 69, No. 4, 2066–2070, 2022, doi: 10.1109/TCSII.2021.3139008.